LA-UR-15-26315 (Accepted Manuscript)

Containment system for experiments on radioactive and other hazardous materials in a Paris-Edinburgh press

Jacobsen, Matthew
Velisavljevic, Nenad

To be published in: Review of Scientific Instruments

DOI to publisher's version: 10.1063/1.4935830

Permalink to record: http://permalink.lanl.gov/object/view?what=info:lanl-repo/lareport/LA-UR-15-26315

Containment System for Experiments on Radioactive and Other Hazardous Materials in a Paris-Edinburgh Press

M.K. Jacobsen[1, a)] and N. Velisavljevic[1]
Shock and Detonation Physics Group (M-9), Los Alamos National Laboratory, Los Alamos, NM 87544 USA

(Dated: 3 November 2015)

Recent technical developments using the large volume Paris-Edinburgh press platform have enabled x-ray synchrotron studies at high pressure and temperature conditions. However, its application to some materials of interest, such as high hazard materials that require special handling due to safety issues, reactivity, or other challenges, has not been feasible without the introduction of special containment systems to eliminate the hazards. However, introduction of a containment system is challenging due to the requirement to provide full safety containment for operation in the variety of environments available, while not hindering any of the experimental probes that are available for inert sample measurement. In this work, we report on the development and implementation of a full safety enclosure for a Paris-Edinburgh type press. During the initial development and subsequent application stage of work, experiments were performed on both cerium dioxide (CeO_2) and uranium (U). This device allows for full implementation of all currently available experimental probes involving the Paris-Edinburgh press at the HPCAT sector of the Advanced Photon Source.

PACS numbers: 64.20.-x,62.50.-p,64.60.A-,81.70.Cv

I. INTRODUCTION

High pressure platforms are important in order to investigate material properties when exposed to large applied stresses. Insight into properties at these conditions is vital for understanding behavior in applications away from ambient conditions, providing a better understanding of structural, electronic, and mechanical properties. Particular uses of this information can be found in the synthesis of possible super-hard materials[1], the enhancement of our knowledge of superconductivity and magnetism[2–4], and material engineering[5,6].

One platform that provides a broad range of experimental data to address these questions is the Paris-Edinburgh press (PE press), which has more recently been coupled with synchrotron x-ray sources to allow x-ray diffraction (XRD), radiography, ultrasonic interferometry (UI), and viscosity probes to be developed[7]. However, due to safety concerns and associated regulations, up to now these measurements could only be performed on inert materials. In order to extend to more sensitive samples, such as radioactive materials, the development of a containment system becomes a necessity.

This system must satisfy two criteria, in that it must (1) comply with safety regulations imposed by the host facility and (2) be fully compatible with the experimental capabilities available for standard/inert material experiments. To address this, we have developed and tested a containment vessel that meets these criteria, as will be described in this remainder of this publication. Test experiments have been performed on CeO_2, an inert material used as a calibration standard at synchrotron sources. Subsequent experiments performed with this vessel were accomplished on radioactive depleted uranium.

[a)] mjacobsen@lanl.gov

II. CONTAINMENT VESSEL FOR RADIOACTIVE MATERIALS

The containment vessel is developed to fit within the functional volume of the PE press (68 mm tall by 95 mm diameter) and is shown in Figures 1 and 2. The basic design concept of any containment vessel for use in high pressure experiments, such as for gas loading of samples[8–10], consists of a portable external can, with lateral ports for x-ray/neutron/optical/etc. access. The anvils are actuated by a t-shaped piston with a tungsten carbide (WC) insert to support the anvils. One anvil is placed on top of this piston with the sample assembly (Figure 3) and an inverted opposed anvil is placed on top to complete the experimental assembly. The assembly is closed using a buttress-threaded top insert.

As the primary function of this insert is the containment of radioactive and hazardous materials, ensuring containment was of the utmost importance in the design process. However, it is additionally important to not impair any of the experimental functionality. Ultrasonic studies require the entrance of an electronic signal for a transducer in the setup[7]. While the piezoelectric transducer could simply be mounted on the outside of the container lid, doing so will substantially lengthen the propagation pathway and cause attenuation of the ultrasound signal. As such, it was necessary to move the transducer closer to the sample without compromising the strength of the setup. This has been achieved via a custom WC insert with a threaded hole to allow passing through of electrical connections.

In this instance, the primary containment along the

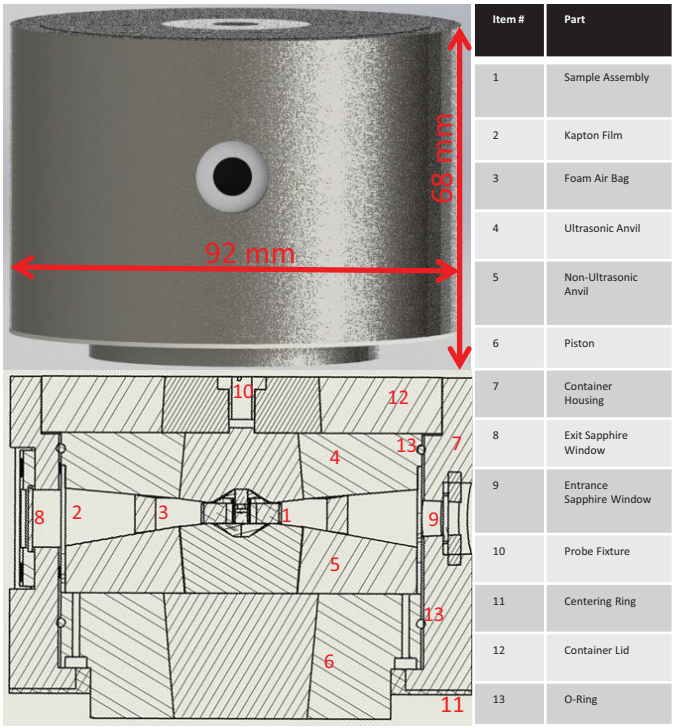

Item #	Part
1	Sample Assembly
2	Kapton Film
3	Foam Air Bag
4	Ultrasonic Anvil
5	Non-Ultrasonic Anvil
6	Piston
7	Container Housing
8	Exit Sapphire Window
9	Entrance Sapphire Window
10	Probe Fixture
11	Centering Ring
12	Container Lid
13	O-Ring

FIG. 1. The containment vessel is, overall, 92 mm in diameter and 68 mm in height, when fully assembled. The entire fixture is comprised of 13 elements, delineated in the table on the right and indicated in the section view at the bottom left. The functions of each part are described in the text. (Color online.)

beam path is comprised of 1 mm thick sapphire windows. These windows are either screwed (downstream) or threaded (upstream) in place. Sapphire was chosen primarily for its high compressive and flexural strength[11], in addition to its transparency in the x-ray regime. While the majority of containment is achieved by the external can and sapphire windows, the Advanced Photon Source (APS) requires as many as three layers of containment for some radioactive materials. Thus, internal containment has been added, in the form of a Kapton barrier around the anvil perimeters. Additionally, the perimeter of the piston and ultrasonic anvil have had o-ring seals included to preclude leakage of material vertically out of the setup and an additional layer of Kapton tape is used on the outside of the window ports. These containment steps are illustrated in the schematic (Figure 1). One final safety precaution in the form of the foam "air bag" component was instituted. As with any larger volume apparatus, concern during experiments with a PE press is on sample failure due to pressure-temperature increase. As such, all safety layers are introduced to impede, diver, or stop any projectile components from penetrating the sapphire windows. In this case, the annular shape completely surrounds the sample assembly and is likely to divert particulates off of the window directions.

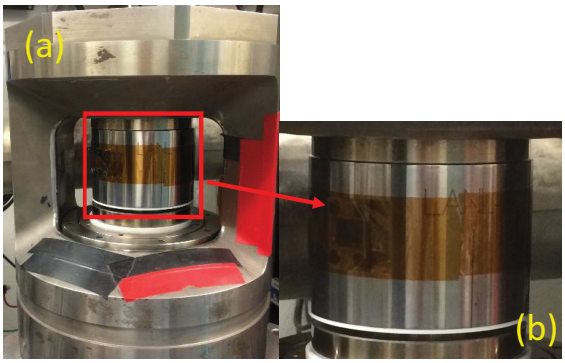

FIG. 2. The insert described in this work has been tested online ((a) and (b)) in the PE press installed at beamline 16-BM-B at the Advanced Photon Source. As stated in the text, the overall dimensions are easily accommodated in the VX-3 model press. (Color online.)

III. EXPERIMENTAL DETAILS

Initial testing has been undertaken at the 16-BM-B beamline (High Pressure Collaborative Access Team, HPCAT) to evaluate the effectiveness of the containment vessel. The goal of this testing is to (1) evaluate the safety of the containment setup and (2) test the compatibility with existing experimental techniques. Testing was first performed on cerium dioxide (ceria, CeO_2) with depleted uranium studied second.

The ceria sample was obtained in pre-compacted pellet form (American Elements, 80% theoretical density, 99.5% purity) with an external diameter of 1.5 mm and thickness of 0.8 mm. Uranium was prepared in house at Los Alamos in pellet form of 0.8 mm diameter and 0.5 mm thick (≈95% theoretical density, 97.6% purity). In both cases, samples were prepared with surfaces better than 1 μm surface roughness. Standard HPCAT 13 mm cell designs were used, as shown in Figure 3. In this, the sample is faced on the top and bottom by an alumina (Al_2O_3) buffer rod and contained around the perimeter by an MgO ring, used for diffractive pressure determination[12]. The remainder of the cell setup is shown in Figure 3.

Samples are monitored *in situ* with x-ray radiography, diffraction, and ultrasonic interferometry. As described in Kono *et al.*[7], the sound velocities of each sample were determined from the radiographic sample length, using the image contrast as shown in Figure 4, and determination of the ultrasonic transit time. Radiographic data was analyzed through an automatic contrast searching function in Igor Pro[13], using initial estimates for the sample top and bottom edges at both ends. A vertical search is performed to find the midpoint in the contrast transition and those points along each surface are mapped, followed by a least squares fit with correlated slopes between the two surfaces to get the best fit linear distance between them. Errors from this fit determine the error in the length value, which is typically 1% or less of the

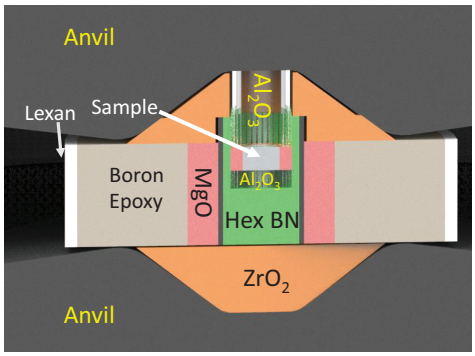

FIG. 3. Samples studies in this setup are contained within a standard 13 mm cell assembly, as described in the text. For the determination of ultrasonic sound velocities, the sample is placed between two alumina (Al_2O_3) buffer rods, which have been polished on both ends. Sound waves are generated from the backside of the top anvil, creating the generator pulse indicated in the plot on the right. Reflections in this assembly are generated at all mated faces between dense materials (i.e. not compressed powder). (Color online.)

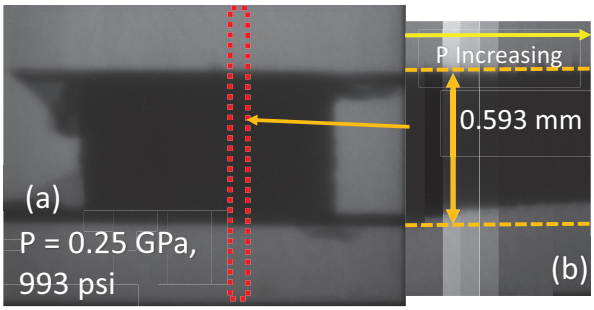

FIG. 4. Sample length is determined from radiographic images of the uranium sample during the experimental run. The left (a) panel shows a sample radiograph with the sample clearly appearing as a black mass and was collected when just enough pressure had been applied to close the initial air space and demonstrate ultrasonic reflections. The red box indicated the segmented region included in the right (b) panel, where some sample segments have been taken from images spanning the whole pressure range studied. Vertical arrows and horizontal lines in this indicate the initial sample dimension and the arrow at the top indicates increasing pressure. The method used to determine sample length is described in the text. (Color online.)

length value. Specific details of the UI technique are presented elsewhere[7]. Error in the travel time is determined by the minimum point spacing, which is 1 ns.

IV. RESULTS

A. Sample Results

For both samples, the determined sound velocities are shown here to illustrate the effectiveness of this setup.

TABLE I. Ambient pressure sound velocities and pressure trends for ceria and uranium to 6 GPa, as determined by linear regression of the resulting data. Errors in these parameters are shown in parentheses after the least significant digit.

Sample	ν_p (km/s)	$\frac{\partial \nu_p}{\partial P}$ (km/GPa-s)	ν_s (km/s)	$\frac{\partial \nu_s}{\partial P}$ (km/GPa-s)
CeO_2	6.401(3)	0.049(1)	3.400(1)	0.017(1)
U	3.402(2)	0.027(1)	1.979(1)	0.026(1)

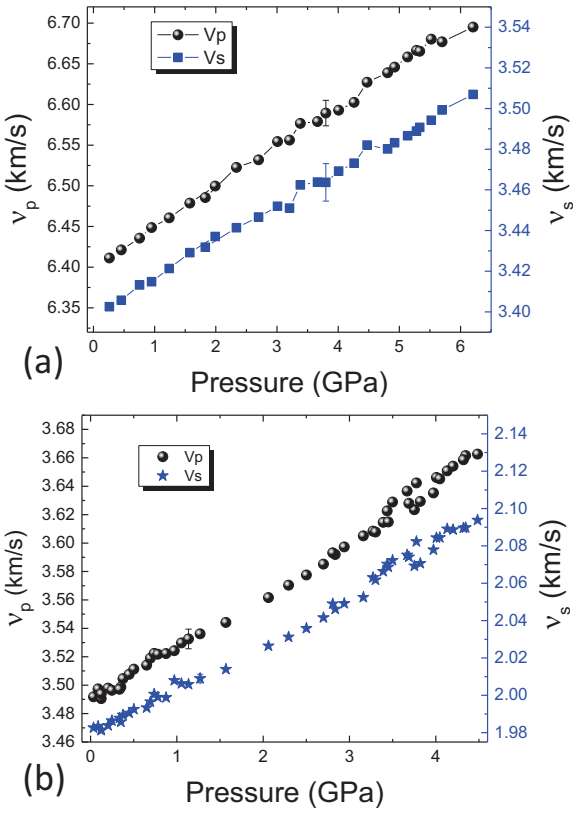

FIG. 5. Measured sound velocities for CeO_2(top) and U(bottom), with the compressional and shear waves (p and s, respectively) shown for each. Both samples show a steady increasing linear trend with applied load up to a maximum of 6 GPa and the ambient pressure values agree well with previous theoretical or experimental values. Representative errors are shown for each set of data. (Color online.)

These results cover pressures up to approximately 6 GPa and linear fits determine both ambient sound velocities and the pressure trend for these parameters. Both are shown in Table I, with plots of the resulting sound velocities shown in Figure 5.

Only theoretical estimations of the sound velocity have been found in the literature for ceria. Kanchana *et al.*[14] reported sound speeds in the range of 6.366 - 6.876 km/s for compressional velocities and 3.360-3.579 km/s for the shear results. For uranium, previously reported sound velocites[15–17] range from 3.18 - 3.54 km/s for compressional and 1.77 - 2.15 km/s for shear. More detail for

both samples will be presented in later reports.

B. Functionality Tests

One consideration to take into account when using inserts, such as the one developed here, is whether the additional safety components introduce restrictions on the experimental techniques. From this work, we have demonstrated that the implementation of UI and radiography is not restrictive. However, the diffractive measurements have limitations. To test these limitations, the detector angle has been swept in 8° increments from 7° to 31° in two-theta space. This has shown that the insert assembly allows diffraction up to 30°, with the lower limit (7°) being imposed by instrumentation aside from the PE press.

Further, in looking forward to future experiments and technique development, we also have to consider if the containment vessel puts any constraints on the P performance of the PE press. Based on previous reports, the cell assembly used is capable of reaching a maximum sample pressure of 7 to 8 GPa[18]. The maximum sample pressure of 6 GPa/4.5 GPa reached for CeO_2/U experiments corresponds to a hydraulic load of 9,000/5,500 psi, with the maximum pressure for the hydraulic line being 11,000 psi. Based on this, the insert does not seem to affect the pressure efficiency of the PE press in which it is used.

C. Safety Evaluation

With regard to the safety of the containment system, the most pressing issue is the failure of the sample assembly (Fig. 3) and the resulting dispersion of the associated parts. To proceed with safety analysis of failure of the sample assembly, any projectile poses a threat due to impact with the sapphire windows, which are the weakest points in the containment assembly, and must be considered in detail. The sample, with its surrounding assembly, is contained between the metal anvils and compressed in an axial direction. As such, any failure of the assembly can only lead to dispersion in a radial direction, away from the compression axis. Sudden failure would then result in all of the compressive stored energy in the assembly converting to kinetic energy of the particulates. To calculate the stored energy, we first look at the macroscopic volume change associated with the applied pressure. This was done for both samples tested in this work, starting with evaluating the radiographic volume as a function of pressure. For the blow-outs considered here, the entire sample is considered to become a projectile.

For both samples (CeO_2 and U) the sample diameter was found to remain unchanged with increasing pressure. Therefore, the volumetric change was primarily due to thickness reduction. Volumes for the cylindrical samples were calculated and then the pressure was plotted as a function of the volume (i.e. P(V)). The energy stored in the sample due to compression was computed as

$$E = -\int_{V_i}^{V_f} P(V)dV \tag{1}$$

The worst case scenario would occur if all of this stored energy were converted to kinetic energy and a free flight path was available for a projectile to travel. In this case, the projectile velocity would be $v = \sqrt{\frac{2*E}{m}}$, which then needs be reduced due to drag from the air and foam regions between the cell assembly and the sapphire window. Exponential reduction is considered in the form of

$$v_f = v_0 e^{\frac{-C_d A \rho x}{2m}} \tag{2}$$

where C_d is the drag coefficient, A is the cross-sectional area of the projectile, ρ is the density of the barrier, m the mass of the projectile (half-mass of sample), and x the path distance traveled. The drag coefficient is obtained from references for a side on cylinder[19]. This provides a final velocity at the window for the projectile under the worst possible case. Results of this computation are presented in Table II.

While such velocities are relatively high, it is necessary to evaluate such impacts through shock results on sapphire, as discussed in a book by Dobrovinskaya *et al.*[20]. In this, they state that the maximum loading rate for sapphire can reach 10.4 to 11.4 km/s. As this is several orders of magnitude higher than the projectile velocity, it

TABLE II. The parameters used in the calculation of the projectile velocity at the sapphire window, along with the resulting values for each step of the calculation. Results are presented for both the CeO_2 and U samples, as well as an extrapolation of the U data to 10 GPa. Standard values, such as air (1.225 km/m^3) and pipe foam (50 km/m^3) density are widely available. Internal distances are 28 mm for the air length and 6 mm for the foam length along projectile paths. Initial thicknesses were for the sample prior to compression and final thicknesses were for samples at the maximal pressure reached. Safety margins presented in this table are ratios of the maximum loading speed of sapphire (assumed at the low end of the range in the text - 10.4 km/s) versus the projectile velocity.

Property	CeO_2	U (4.5 GPa)	U (10 GPa[a])
Diameter (μm)	1536.9	783.3	783.3
Initial Thickness (μm)	966.5	544.5	544.5
Final Thickness (μm)	684.9	427.2	422.9
m (mg)	10.8	4.8	4.8
C_d	1.53	1.18	1.53
A (10^6 m^2)	1.05	0.335	0.330
E (J)	1.095	0.045	0.577
v_i (m/s)	450	137	490
v_f (m/s)	449	137	477
Safety Margin	23	76	22

[a] Extrapolated from 4.5 GPa data

is unlikely that such a projectile will inflict sufficient damage to rupture the window. A different material could be used for this purpose, SiO_2 for example at the expense of the safety margin (max loading rate of approximately 5.2 km/s). Considering the potential impact of a ruptured window, it seemed reasonable to err on the side of caution and have a larger safety margin. Further support for this analysis comes from reported testing of sapphire for armor materials[21], where varying thicknesses were subjected to ammunition impact. In this, they found that the sapphire plates tested could routinely survive several impacts of armor piercing rounds without penetration. Since the masses of sample used here are orders of magnitude smaller (masses of bullets on the order of grams) and not designed to penetrate, a correspondingly smaller window is likely to survive in a similar fashion. During experimentation, however, no blow-outs occurred. As such events typically occur when such systems are subject to combined pressure and temperature testing, further evaluation of the containment safety is planned when temperature measurement and heating are implemented in the setup. Further, considering the approximations made in the course of the calculation, the reported safety margin is a gross under-estimation of the actual safety margin. For example, all compressive energy is assumed to be stored and consumed as motion of the projectile, which would be the case if no other material surrounded the sample and, upon release, the sample had a free flight path in the axial direction. In reality, the only dispersion possible is in the radial direction, with most of the energy consumed in plastic deformation of the sample assembly materials.

In contrast to this picture, failure typically involves a relatively small burst with some ejected powder sample. If the sample is assumed to be comprised of 1 μm diameter spherical grains, it can easily be demonstrated that the "air bag" component will successfully stop the ejected powder. For this analysis, we take the extrapolated uranium data as our starting point. At 10 GPa, the sample will have a volume of approximately 0.2038 mm^3. A 1μm sphere will have a total volume of 0.5236 μm^3, giving a total composition of 1.47 gigaparticles. Overall, this has little effect on the departure velocity of any one particle, assuming the energy evenly dispersed over the particles. However, when drag is considered from any one particle due to the foam, the resulting velocity at the outlet of the foam is 0.159 μm/s, suggesting the foam effectively stops such particulates.

V. CONCLUSIONS

In conclusion, we demonstrate successful development, testing, and application of a containment vessel for experimentation on radioactive and other sensitive materials. The goal in developing the containment vessel is to ensure that the full range of experimental capabilities, namely ultrasonic sound velocity determination with concurrent x-ray diffraction and radiography under pressure and temperature, are fully accessible for studying higher sensitivity materials. Compatible with the currently existing Paris-Edinburgh press system available at the HPCAT sector of the Advanced Photon Source, this insert implements three containment barriers to encapsulate the sample and allow safe high pressure experimentation. Its design has considered the needs required for implementation of all three techniques listed above, but also to allow the flexibility to add new experimental techniques as needed. Demonstration of the effectiveness of this design has been carried out by experimentation on both inert ceria and radioactive depleted uranium.

From the results of these tests, sound velocities have been determined for both samples up to 6 GPa. In both cases, the ambient pressure sound velocities have been found in agreement with either theoretical or experimentally determined values from references. Functionality testing has been performed and illustrates that neither the radiographic or ultrasound techniques are limited by implementation of the insert. In contrast, diffraction is restricted to the angular range from 7 to 30 degrees, in part from external instrumentation, which is acceptable for most studies. Either minimal or negligible loss of pressure range is found when compared with the original PE press[18] performance on a 13 mm cell. Further improvements to this device are currently in development or planned in the near future, including heating and temperature measurement capacities.

ACKNOWLEDGMENTS

Los Alamos National Laboratory (LANL) is operated by LANS, LLC for the DOE-NNSA under contract no. DE-AC52-06NA25396. Work was in part supported by LANL Science Campaign 2. Portions of this work were performed at HPCAT (Sector 16), Advanced Photon Source (APS), Argonne National Laboratory. HPCAT operations are supported by DOE-NNSA under Award No. DE-NA0001974 and DOE-BES under Award No. DE-FG02-99ER45775, with partial instrumentation funding by NSF. Use of the Advanced Photon Source, an Office of Science User Facility operated for the US Department of Energy (DOE) Office of Science by Argonne National Laboratory, was supported by the US DOE under Contract No. DE-AC02-06CH11357. MKJ gratefully acknowledges the support of the U.S. Department of Energy through the LANL/LDRD Program and the G.T. Seaborg Institute for this work. The authors also thank Professor Baosheng Li for the use of his pulse-echo overlap software for determination of transit times.

[1] M. Weinberger, S. Tolbert, and A. Kavner, Physical Review Letters **100**, 045506 (2008).

[2] M. Nakashima, Y. Haga, E. Yamamoto, Y. Tokiwa, M. Hedo, Y. Uwatoko, R. Settai, and Y. Onuki, Journal of Physics-Condensed Matter **15**, S2007 (2003).

[3]N. Tateiwa, S. Ikeda, Y. Haga, T. D. Matsuda, M. Nakashima, D. Aoki, R. Settai, and Y. Onuki, Journal of Physics: Conference Series **150**, 042206 (2009).
[4]D. Vangennep, *Charge density waves and superconductivity in alpha-uranium*, Ph.D. thesis, Florida State University (2012).
[5]E. Hinteregger, K. Wurst, L. Perfler, F. Kraus, and H. Huppertz, European Journal of Inorganic Chemistry , 5247 (2013).
[6]G. Parakhonskiy, N. Dubrovinskaia, E. Bykova, R. Wirth, and L. Dubrovinsky, High Pressure Research **33**, 673 (2013).
[7]Y. Kono, C. Park, T. Sakamaki, C. Kenny-Benson, G. Shen, and Y. Wang, Review of Scientific Instruments **83**, 033905 (2012).
[8]A. Bocian, C. L. Bull, H. Hamidov, J. S. Loveday, R. J. Nelmes, and K. V. Kamenev, Review of Scientific Instruments **81**, 093904 (2010).
[9]A. Bocian, *Gas-loading apparatus for large-volume high-pressure cell*, Ph.D. thesis, University of Edinburgh (2012).
[10]S. Klotz, J. Philippe, C. L. Bull, J. S. Loveday, and R. J. Nelmes, High Pressure Research **33**, 214 (2013).
[11]Swiss Jewel, "Physical Properties of Synthetic Sapphire," (2000).
[12]S. Speziale, C.-S. Zha, T. S. Duffy, R. J. Hemley, and H.-K. Mao, Journal of Geophysical Research **106**, 515 (2001).
[13]WaveMetrics, "Igor Pro," (2015).
[14]V. Kanchana, G. Vaitheeswaran, A. Svane, and A. Delin, Journal of Physics: Condensed Matter **18**, 9615 (2006).
[15]H. L. Laquer, Nuclear Science and Engineering **5**, 197 (1959).
[16]M. Boivineau, L. Arles, J. M. Vermeulen, and T. Thevenin, Physica B: Condensed Matter **190**, 31 (1993).
[17]J. Bouchet and R. C. Albers, Journal of Physics: Condensed Matter **23**, 215402 (2011).
[18]A. Yamada, Y. Wang, T. Inoue, W. Yang, C. Park, T. Yu, and G. Shen, Review of Scientific Instruments **82**, 10 (2011).
[19]P. W. Cooper, *Explosives Engineering* (Wiley-VCH Verlag GmbH & Co. KGaA, 1996).
[20]E. R. Dobrovinskaya, L. A. Lytvynov, and V. Pishchik, *Sapphire: Material, Manufacturing, Applications* (Springer Science and Business Media, 2009) p. 480.
[21]J. Rioux, C. Jones, M. Mandelartz, and V. Pluen, Advanced Materials and Processes **225**, 31 (2007).